

Adaptive Fault Tolerant Control Design for a Model of DC-X Dynamics*

Jovan D. Bošković, Joseph A. Jackson and Raman K. Mehra

Scientific Systems Company, Inc., 500 W. Cummings Park, Suite 3000, Woburn, MA 01801

Nhan T. Nguyen

NASA Ames Research Center, MS 269-4, Moffet Field, CA 94035-1000

Abstract—A Failure Detection, Identification and Reconfiguration (FDIR) control scheme is developed for a dynamic model of the Delta Clipper–Experimental (DC-X) single stage to orbit rocket concept. The six degree of freedom, redundantly actuated model provides a well-suited test case for designing a fault-tolerant controller for actuators with different response rates. The reconfigurable controller maintains the desired closed-loop performance. Robustness of the system was demonstrated under a large number of different single and multiple failure cases.

I. INTRODUCTION

The on-board Failure Detection Identification and Reconfiguration (FDIR) problem is particularly important for space exploration vehicles which require minimal down-time for repairs during a mission. Our focus has been on the Delta Clipper Experimental (DC-X), [1]-[4], which was designed by McDonnell-Douglas in the early 1990s as a one-third scale prototype for a proposed vertical take-off and landing (VTOL) reusable launch vehicle capable of single stage to orbit (SSTO).

This work presents an adaptive reconfigurable flight control design for a DC-X control design model, consisting of translational and attitude dynamics, four gimballed engines, four reaction control system (RCS) thrusters for attitude control, and actuator dynamics with position and rate limits. A variety of failures were injected into the model, and our modified FDIR system, discussed in [7], [8] and described below, was implemented and tested to evaluate the overall system performance. Special consideration was given to determining the total number of failures that can be accommodated using the available actuator redundancy.

We have recently modified our baseline Fast on-Line Actuator Reconfiguration Enhancement (FLARE) system to include a new failure parametrization [5], as well as a multiple model-based FDI similar to that from [10]. Central to FLARE, Fig. 1, are FDI observers based on the new failure parametrization that describes a large class of failures in terms of a single uncertain parameter. A previous version of FLARE was successfully tested under severe flight critical failures on a piloted simulator at Boeing resulting in robust failure accommodation and excellent overall performance [7]. The FLARE system achieves very fast detection and identification of failures in flight control actuators, and effective control reconfiguration in the presence of single

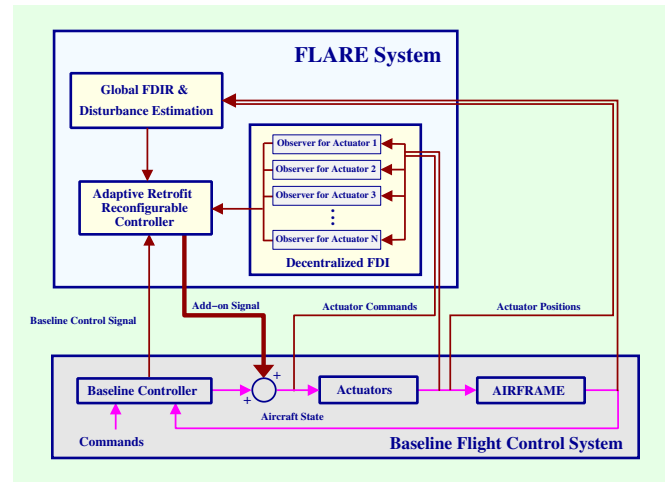


Fig. 1. Structure of the Fast on-Line Actuator Reconfiguration Enhancement (FLARE) System (©1999-2005 Scientific Systems Company, Inc.)

or multiple actuator failures and control effector damages even while rejecting external disturbances. The FLARE system combines different FDIR algorithms with a disturbance rejection mechanism within a retrofit control architecture. In collaboration with Boeing Phantom Works, the performance of the previous version of FLARE system was extensively evaluated using high-fidelity and piloted simulators. The FLARE system achieved excellent response in the presence of severe flight-critical control effector failures, and received excellent HQ ratings from the pilot. The FLARE system was used as a basis for FDIR design in the context of the DC-X model.

The sections that follow describe the plant and actuator dynamic model, trajectory design, failure injection, reconfigurable control design, and simulation results.

II. DC-X MODEL REPRESENTATION

The DC-X is propelled by four liquid-propelled engines and controlled by electro-mechanical actuators (EMAs) driving two gimbal angles for each engine and four RCS thrusters. The basic schematic for the vehicle is shown in Fig. 3.

For each engine, three control inputs are available: thrust magnitude (T), radial gimbal angle (α_R) and tangential gimbal angle (α_T). The radial gimbal angle is measured

*This work was supported by NASA under contract #NNAAA04C to SSCI.



Fig. 2. (credit:NASA) The Delta Clipper-Experimental at take-off.

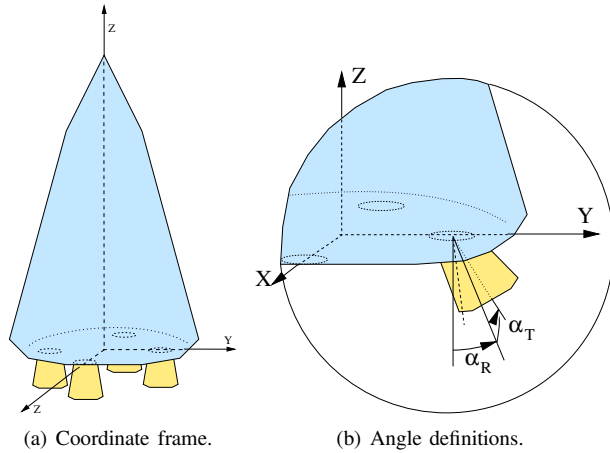


Fig. 3. (a) The DC-X is a VTOL type vehicle, designed as a reusable SSTO rocket. (b) The control inputs for each engine are thrust (T), radial gimbaling angle (α_R) and tangential gimbaling angle (α_T).

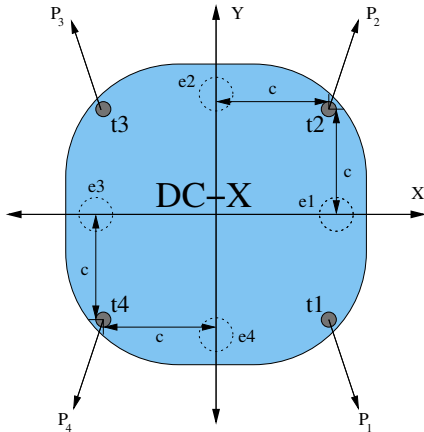


Fig. 4. The RCS thrusters are designed to control the vehicle's attitude. The thrusters are primarily used for roll and pitch angle control. Here $e_1 \dots e_4$ denote the locations of the engines, while $t_1 \dots t_4$ denote RCS thrusters.

positive outward from the craft, while the tangential gimbaling angle is measured positive counter-clockwise when looking from the nose toward the base of the vehicle. The four engines are numbered, beginning with the engine along the x -axis being engine one, with two through four proceeding counter-clockwise around the perimeter of the vehicle.

Based upon angular definitions in Fig. 3, the forces acting

on the body can be calculated as follows:

$$\begin{aligned} F_{xe1} &= -T_1 \sin \alpha_{R1}, & F_{ye1} &= -T_1 \cos \alpha_{R1} \sin \alpha_{T1}, \\ F_{xe2} &= T_2 \cos \alpha_{R2} \sin \alpha_{T2}, & F_{ye2} &= -T_2 \sin \alpha_{R2}, \\ F_{xe3} &= T_3 \sin \alpha_{R3}, & F_{ye3} &= -T_3 \cos \alpha_{R3} \sin \alpha_{T3}, \\ F_{xe4} &= -T_4 \cos \alpha_{R4} \sin \alpha_{T4}, & F_{ye4} &= T_4 \sin \alpha_{R4}, \\ F_{zei} &= T_i \cos \alpha_{Ri} \cos \alpha_{Ti}, & & \text{for } i = 1, 2, 3, 4. \end{aligned} \quad (1)$$

The RCS thrusters are installed so that all resultant forces are applied in the x - y plane of the body frame. Hence, the thrusters are used for attitude control. The resultant thrust vectors from the RCS are designed primarily to give a greater amount of torque to the pitch and roll of the vehicle. The thrusters also produce minimal yaw moment on the vehicle, since the resultant vector from each thruster is not incident upon the vehicle's center of gravity.

The contributions of each thruster to the total force acting on the vehicle is calculated as:

$$F_{xti} = d_{xi} P_i, \quad F_{yti} = d_{yi} P_i, \quad i = 1, 2, 3, 4,$$

where d_{xi} and d_{yi} are the components of RCS along the body frame x and y axes, respectively, and P_i are the thrust magnitudes from each RCS thruster.

For the representation of the plant, the forces are grouped according to the coordinate axis along which they are applied to yield the net force in each direction in body coordinates. Assuming a vertical world-frame orientation, the component force due to gravity is in the negative z direction. The elements of the force vector $F = [F_x \ F_y \ F_z]^T$ are expressed as sums of forces from the engines and RCS thrusters:

$$\begin{aligned} F_x &= \sum_{i=1}^4 (F_{xei} + F_{xti}), & F_y &= \sum_{i=1}^4 (F_{yei} + F_{yti}), \\ F_z &= \sum_{i=1}^4 (F_{zei} + F_{zti}) - mg. \end{aligned} \quad (2)$$

Torque is defined by $\tau_i = r_i \times F_i$, with $\tau_i = [\tau_{xi} \ \tau_{yi} \ \tau_{zi}]^T$. Given the lateral and longitudinal distances, a and b , respectively, from the center of gravity to the point where the engine thrust exerts forces on the vehicle, the cross products representing the torques from the four engines about principle axes result in

$$\begin{aligned} \tau_{xe} &= bF_{ye1} + bF_{ye2} + aF_{ze2} + bF_{ye3} + bF_{ye4} - aF_{ze4}, \\ \tau_{ye} &= -bF_{xe1} - aF_{ze1} - bF_{xe2} - bF_{xe3} + aF_{ze3} - bF_{xe4}, \\ \tau_{ze} &= aF_{ye1} - aF_{xe1} - aF_{ye3} + aF_{xe4}. \end{aligned}$$

If c and d represent the lateral and longitudinal distances from the thrusters to the center of gravity, then the sum of the torques from the four thrusters can be computed as

$$\begin{aligned} \tau_{xt} &= -dF_{yt1} - dF_{yt2} - dF_{yt3} - dF_{yt4}, \\ \tau_{yt} &= dF_{xt1} + dF_{xt2} + dF_{xt3} + dF_{xt4}, \\ \tau_{zt} &= -cF_{xt1} + cF_{yt1} - cF_{xt2} + cF_{yt2} \\ &\quad -cF_{xt3} + cF_{yt3} - cF_{xt4} + cF_{yt4}. \end{aligned} \quad (3)$$

The overall torque about each body frame axis is simply the sum of the torque from the engines in (3) and the torque from the thrusters in (3).

Let the attitude dynamics be of the form $J\dot{\omega} = \sum \tau$, where, due to small-angle approximation, we assume that $\omega = [\phi \ \theta \ \psi]^T$ and that the Coriolis term $\omega^\times J\omega$ can be neglected. The system's position and attitude dynamics are now of the form:

$$\begin{aligned} \ddot{x} &= \frac{1}{m}F_x, & \ddot{y} &= \frac{1}{m}F_y, & \ddot{z} &= \frac{1}{m}F_z, \\ \dot{\phi} &= \frac{1}{J_{xx}}\tau_x, & \dot{\theta} &= \frac{1}{J_{yy}}\tau_y, & \dot{\psi} &= \frac{1}{J_{zz}}\tau_z. \end{aligned} \quad (4)$$

The attitude dynamics are simplified since the control objective is to maintain the Euler angles close to zero.

III. CONTROL DESIGN ASSUMPTIONS

Assumptions for control design include the following: the desired reference model has second order dynamics, the actuators have a first order response, the trajectory is generally constant acceleration, and the faults are lock in place, hard-over, and loss of effectiveness.

A. Reference Model Design

Our test maneuver follows a basic climb, x and y translation, then descend path. The desired closed-loop dynamics along the z -axis are of the form:

$$\ddot{z} = -k_2(\dot{z} - \dot{z}^*) - k_1(z - z^*) + \ddot{z}^*, \quad (5)$$

where \dot{z}^* , z^* , and \ddot{z}^* represent the desired velocity, position, and acceleration. Each of the relationships in (4) has an associated equation of the form in (5).

Since the plant for the DC-X dynamic model is non-affine in its inputs, tracking the above desired dynamics cannot be achieved in a straightforward way. However, another derivative of the system dynamics can be taken resulting in the *derivative of the control input* appearing linearly in the dynamic equation [9]. This results in a higher-order reference model that can be tracked, and is of the form:

$$\ddot{p}^* = -k_3\dot{p}^* - k_2\dot{p}^* - k_1p^* + k_1r, \quad (6)$$

where $p^* = [x \ y \ z \ w_1 \ w_2 \ w_3]^T [x^* \ y^* \ z^* \ 0 \ 0 \ 0]^T$, and r denotes the command input which is zero for w_i . We define

$$\eta^* = -k_3\dot{p}^* - k_2\dot{p}^* - k_1p^* + k_1r, \quad (7)$$

as the desired system dynamics.

B. Fault Insertion

Three basic actuator fault modes are included in the simulation. These include: (i) Lock in Place (LIP) ($u(t)$ is locked at its current position); (ii) Hard-over ($u(t)$ locks at the position limit); and (iii) Loss of Effectiveness (actuator gain decreases from $k = 1$ to a value $k \in (0, 1)$).

To simulate engine or gimbal failures, an appropriate failure model is needed. First, a LIP matrix Σ is defined as $\Sigma = \text{diag}([\sigma_1 \ \sigma_2 \ \dots \ \sigma_m])$, where $\sigma_i(t) = 1$ for $t < t_{Fi}$, and $\sigma_i(t) = 0$ for $t \geq t_{Fi}$. This matrix is initialized to an $m \times m$ identity matrix, where m is the number of control inputs. When a LIP failure occurs at the j -th input, the value at $\Sigma(j, j)$ is set to zero. For convenience, the value

at $\Sigma(j, j)$ will also be referred to as σ_j . To include LOE within the model, an Input Effectiveness Matrix K is chosen as a diagonal matrix whose elements describe effectiveness of each control input. K is also initialized as an $n \times n$ identity matrix.

Now the actuator dynamics including the failure model is of the form:

$$\dot{\mathbf{u}} = \Lambda_a[(\mathbf{u} - \mathbf{K}\mathbf{u}_c) + (\mathbf{I} - \Sigma)\mathbf{u}], \quad (8)$$

where \mathbf{u}_c is the controller output, \mathbf{u} is the output of the actuator, $\Lambda_a = \text{diag}[\lambda_{a1} \ \lambda_{a2} \ \dots \ \lambda_{am}]$ is the matrix of actuator gains, and $K = \text{diag}([k_1 \ k_2 \ \dots \ k_m])$, where $k_i \in [\epsilon_i, 0]$, and $\epsilon_i \ll 1$.

IV. FAILURE DETECTION AND IDENTIFICATION

The algorithms for estimating the unknown failure-related parameters associated with DC-X actuators are based on the basic FLARE design augmented with the new failure parametrization-based FDI observers, and are given below.

Observer: The observer for the model (8) is based on the new failure parametrization [5] of the form:

$$\dot{\mathbf{u}} = -\Lambda_a\mathbf{u} + \Lambda_a(\Theta\mathbf{u}_c + \Delta\mathbf{u}). \quad (9)$$

where $\Theta = \text{diag}[\theta_1 \ \theta_2 \ \dots \ \theta_m]$,

$$\Delta = \text{diag}\left(\frac{\delta}{\theta_1 + \delta} \quad \frac{\delta}{\theta_2 + \delta} \quad \dots \quad \frac{\delta}{\theta_m + \delta}\right), \quad (10)$$

and $0 < \delta \ll 1$. It is seen that, when $\theta_i = 0$, $\dot{u}_i = 0$. When $\theta_i = \bar{\theta}_i > 0$, we have that $\dot{u}_i \cong \lambda_{ai}(u_i - \bar{\theta}_i u_{ci})$ since $\delta \bar{u}_i / (\bar{\theta}_i + \delta) \cong 0$. Hence the above model has the desired properties of covering both the LIP and LOE cases for a sufficiently small δ .

Now the observer is chosen in the form:

$$\dot{\hat{\mathbf{u}}} = -\Lambda_a\hat{\mathbf{u}} + \Lambda_a(\hat{\Theta}\mathbf{u}_c + \hat{\Delta}\hat{\mathbf{u}}) - \lambda_o\hat{\mathbf{e}}, \quad (11)$$

where $\hat{\mathbf{e}} = \hat{\mathbf{u}} - \mathbf{u}$, $\hat{\Theta} = \text{diag}[\hat{\theta}_1 \ \hat{\theta}_2 \ \dots \ \hat{\theta}_m]$,

$$\hat{\Delta} = \text{diag}\left(\frac{\delta}{\hat{\theta}_1 + \delta} \quad \frac{\delta}{\hat{\theta}_2 + \delta} \quad \dots \quad \frac{\delta}{\hat{\theta}_m + \delta}\right), \quad (12)$$

and $\Lambda_o = \text{diag}[\lambda_{o1} \ \lambda_{o2} \ \dots \ \lambda_{om}]$.

Adaptive laws: Adaptive laws are of the form:

$$\dot{\hat{\theta}}_i = \text{Proj}_{[0,1]}\{-\gamma_i\omega_i\hat{\mathbf{e}}_i\}, \quad \hat{\theta}_i(0) = 1, \quad (13)$$

where $\gamma_i > 0$ denote adaptive gains, and

$$\omega_i = u_{ci} - \frac{\delta u_i}{(\hat{\theta}_i + \delta)(\theta_i + \delta)}.$$

V. CONTROL DESIGN

The reconfigurable control design starts with the design of a baseline controller. The latter is used as a basis for the adaptive controller that at every instant uses estimates generated by an FDI observer. We describe the baseline control design below.

A. Baseline Controller

In the no-failure case the nonlinear state-space model of the DC-X dynamics can be represented in a compact form as:

$$\begin{aligned}\dot{\mathbf{x}}_1 &= \mathbf{x}_2 \\ \dot{\mathbf{x}}_2 &= G_o(\mathbf{u}) + [0 \ 0 \ -g \ 0 \ 0 \ 0]^\top,\end{aligned}\quad (14)$$

where $x_1 = [x \ y \ z \ w_1 \ w_2 \ w_3]^\top$, $x_2 = [\dot{x} \ \dot{y} \ \dot{z} \ \dot{w}_1 \ \dot{w}_2 \ \dot{w}_3]^\top$, and $u \in \mathbb{R}^{16}$. It is seen that the above system can be rewritten as $\dot{\mathbf{x}}_1 = G_o(u) + \bar{g}$.

The actuator dynamics are of the form:

$$\dot{\mathbf{u}} = -\Lambda(\mathbf{u} - \mathbf{u}_c),$$

where $\Lambda = \text{diag}[\lambda_1 \ \lambda_2 \ \dots \ \lambda_m]$ and $\lambda_i > 0$.

Since G_o cannot be inverted analytically, using the approach from [9] we take another derivative of the above equation to obtain:

$$\ddot{\mathbf{x}}_1 = G(\mathbf{u})\dot{u}, \quad (16)$$

where $G = \frac{\partial G_o(u)}{\partial u}$. Assuming that G is invertible on a domain, we design the following dynamic controller:

$$\mathbf{u}_c = u + \Lambda^{-1}G(u)^\top (G(u)G(u)^\top)^{-1} \boldsymbol{\eta}^*. \quad (17)$$

The resulting closed-loop system is simply $\ddot{\mathbf{x}}_1 = \boldsymbol{\eta}^*$. More details regarding the dynamic controller technique in the adaptive control context can be found in [9].

It is interesting to note that, due to the first-order actuator dynamics, the actual control input u_c is static, i.e. there is no need to generate it as a solution of a differential equation since it can be directly computed from (17). In addition, since Λ is known, even when u is not measurable, we can build a simple observer to estimate u , $\hat{u} = \Lambda(\hat{u} - u_c)$ so that, for zero initial conditions, $\hat{u}(t) = u(t)$ for all time.

B. Adaptive Reconfigurable Controller

Now the adaptive reconfigurable controller is chosen in the form:

$$u = (G(u)\hat{\Theta})^\top (G(u)\hat{\Theta}^2 G(u)^\top)^{-1} (\boldsymbol{\eta}^* - \sum_{i=1}^m g_i(x) \frac{\delta u_i}{\theta_i + \delta}).$$

As shown in [5], this control law, in conjunction with the above estimator and adaptive laws, assures closed-loop stability and asymptotic convergence of the tracking error to zero.

VI. SIMULATION SETUP

The high-fidelity DC-X dynamic model describes the relationship between the states of the vehicle and the main engine propulsive thrust, gimballed angles and the RCS thrusters.

For the control design, the fully nonlinear dynamics were linearized about nominal values to help alleviate scaling issues which led to matrix singularity and loss of rank. Nominal input conditions were assumed to be those providing steady hover (gimballed angles and RCS equal to zero, total main engine thrust balancing gravity). A change of coordinates for the main engine thrust and RCS further improved

the conditioning of the controller so all inputs maintained the same order of magnitude. The plant position dynamics remained fully nonlinear, while plant attitude dynamics were approximated by a linear model.

Since the controller was designed to accommodate both loss of effectiveness (LOE) and lock in place (LIP) failures, a test regime of increasingly drastic failures was designed to evaluate the spectrum of faults that the controller could tolerate. The failures were injected at 20 seconds (during the ascent portion of the trajectory) which was expected to be the worst-time-of-failure for this particular trajectory.

Before online failure estimation was included in the simulation, the controller was first validated using known failures. Once the robustness of the scheme was established amid failures, the failure estimators were included in the closed loop and tuned for acceptable performance.

VII. SIMULATION RESULTS

Sample results are presented in Table I. The actuators are numbered 1 through 16, with four main engines, four radial gimballed angles, four tangential angles, and four RCS thrusters, as designated in the schematics, Figs. 3 and 4. For the sake of comparison, the baseline controller utilizing an inverse dynamics control scheme is simulated alongside the reconfigurable controller. The table presents the maximum rotation about each axis, the maximum tracking error, and the final tracking error. Pitch and yaw angles greater than 45 degrees are considered failure.

Failures were introduced to the system both symmetrically and asymmetrically. Figs. 5(a), 5(b) and 5(c) records the states, estimates, and inputs, respectively, for the reconfigurable controller with LIP failures at actuators 1, 5, and 9. The inputs in Fig. 5(d) are from a simulation performed at the theoretical limit of controllability, i.e. we control six degrees-of-freedom using only six actuators (ten actuators are failed). The plots from the other simulations in Table I look very similar to the included results.

VIII. DISCUSSION OF RESULTS

The reconfigurable controller is able to accommodate multiple severe failures, though doing so may exhaust the available control authority. For instance, when the maneuver requires the control authority that is already close to its limit and there are multiple failures, the reconfigurable controller may fail to meet the control objective. In addition, accommodation of hard-over failures require large control authority and reduce the operational envelope. The necessary control authority is not available in DC-X in the case of two or more hard-over failures.

Simulation results and analysis of the plant affirm that the gimballed actuators are linked to specific body-frame translations and rotations. For example, it is apparent that failures of actuator 10 (the 12 o'clock tangential EMA driving angle α_{T2}) are tied to translations in x and yaw rotations. Hence the persistent excitation to adapt the failure parameter on actuator 10 is not available until the trajectory requires the actuator contribute to x -translation. Furthermore, holding a

TABLE I
DC-X LIP AND LOE FAILURE MATRIX RESULTS

Failure Mode		Baseline Controller					Reconfigurable Controller				
Actuators	Failure	Max Angles			Tracking Error		Max Angles			Tracking Error	
		Pitch	Yaw	Roll	Max	Final	Pitch	Yaw	Roll	Max	Final
<i>Lock in Place</i>											
1,5,9	All LIP	2.1	9.4	8.9	22.9	9.4	.5	4.2	0.8	4.1	1.4
5,6,7,8	All LIP	3.3	3.0	0	6.1	3.7	.5	.5	0	3.9	.9
5,6,9,10	All LIP	3.5	3.1	1.0	6.4	3.8	.5	.5	.2	3.9	.9
5,7,9,11	All LIP	3.3	3.0	0	6.1	3.7	.5	.5	0	3.9	.9
1,5,6,9,10	All LIP	4.0	9.8	7.6	23.2	10.8	.4	3.8	1.4	4.1	1.3
1,2,5,6,9,10	All LIP	12.7	13.6	2.7	69.4	21.4	7.7	5.6	.2	6.7	1.9
1,5,6,7,9,10,11	All LIP	8.5	60.8	272.8	278.4	278.4	3.6	5.2	14.3	4.1	.8
1,2,5,6,7,9,10,11	All LIP	17.7	62.0	285.3	272.4	272.4	9.2	5.5	12.8	6.8	2.2
1,2,3,5,6,7,8,11,12	All LIP	9.3	7.3	17.7	162.5	45.9	12.1	1.9	24.1	8.2	2.0
1,2,3,5,6,7,8,11,12,14	All LIP	11.3	20.9	74.7	175.6	50.1	28.6	29.5	45.5	8.2	2.0
1,2,3,5,6,7,8,11,12,15	All LIP	24.7	25.8	113.7	223.2	223.2	12.1	2.1	24.1	8.2	2.0
<i>Lock in Place/Hard Over</i>											
1,5,9	HO(h),LIP,LIP	2.3	33.7	9.9	75.5	41.5	.5	35.2	1.1	13.6	3.4
1,5,9	LIP,HO(h),LIP	2.1	56.2	8.9	26.4	16.5	.5	43.3	1.3	5.1	2.0
1,5,9	LIP,HO(l),LIP	2.1	51.0	8.8	22.1	15.4	.5	50.1	1.1	5.5	2.2
1,5,9	LIP,LIP,HO(h)	57.7	9.4	249.8	26.1	20.9	50.4	3.7	213.1	5.7	2.6
1,5,9	LIP,HO(h),HO(h)	57.1	56.3	249.6	30.5	25.1	56.9	43.1	214.2	6.8	3.8
<i>Loss of Effectiveness</i>											
1,5,9	.5,.5,.5	1.6	3.9	6.0	7.0	5.6	.9	6.4	4.2	4.1	1.5
1,5,9	.25,.5,.75	.7	6.3	2.9	10.6	9.7	.5	2.5	2.1	4.2	1.7
1,5,9	.75,.75,.75	.8	1.8	2.9	4.9	2.6	.5	.8	2.1	3.8	1.1
1,5,9	.25,.25,.25	2.6	6.4	9.5	10.6	9.7	1.2	2.5	6.3	4.2	1.7
1,2,5,9,6,10	.4,.4,.4,.4,.4	5.7	5.7	1.4	15.9	15.8	5.6	3.8	1.6	4.9	2.7
<i>Slow Degradation</i>											
k=2 1,5,9	.5,.5,.5	1.6	3.9	6.0	7.0	5.6	.9	6.4	4.2	4.1	1.5
k=1 1,5,9	.5,.5,.5	1.4	3.9	5.0	7.0	5.6	.6	6.1	2.6	4.1	1.5
k=10 1,5,9	.5,.5,.5	.9	3.9	3.2	7.0	5.5	.6	7.4	3.6	4.1	1.5
k=25 1,5,9	.5,.5,.5	.9	3.8	3.1	7.0	5.5	.6	1.6	4.5	4.1	1.4
<i>HYBRID</i>											
1,5,6,7,9,10,11	LOE@7,11(4)	5.6	10.9	34.3	24.3	18.1	5.0	5.9	15.2	4.0	1.2

command does not provide sufficient persistent excitation for estimate convergence. Trajectories which require continuous motion of inputs to actuators yield more accurate estimates. This concept lends itself to another observation that the vehicle's dynamic response to failure depends largely on the trajectory required for the vehicle: failure of an unused actuator results in no appreciable change in vehicle behavior.

The results organized in Table I indicate that in every case the reconfigurable controller outperformed the baseline controller in terms of tracking the trajectory while maintaining nominal attitude. The assortment of LIP failures resulted in maximum tracking error between 3.9 and 8.2 meters for the reconfigurable controller compared to 6.2 to 278.4 meters maximum error for the baseline controller. In no LOE or LIP cases did the reconfigurable controller violate the acceptable attitude criteria, whereas two of the baseline test cases failed.

Failures of an even more drastic type, such as hard-over actuator failures, have potentially devastating results. Both controllers were able to mitigate a hard-over full throttle engine, though the reconfigurable controller tracked the desired trajectory much better (baseline-75.5 m error, reconfig-13.6 m error). Hard-over failures on the EMA-driven angles result in unacceptable performance in the case of the both controllers. Two hard-over failures cause both controllers to fail.

Amid partially failed actuators, tabulated in the lower half of Table I, our FDIR system is capable of accurately identifying and accommodating the failures. As with the results from LIP failures, the reconfigurable controller outperforms the baseline in all cases. Naturally, failures closer to zero (e.g. 0.25 or less) produce results which resemble LIP failures. Analyzing the speed of performance degradation indicates that the estimators are consistent regardless of the speed of the failure.

As shown in Fig. 5(d), the plant has sufficient redundancy not to saturate the control inputs. With all but six actuators locked into place mid-maneuver, the remaining six actuators maintain six degree-of-freedom trajectory tracking for the rest of the maneuver. The system has 16 actuators, 10 of which are redundant. However, as noted above, this redundancy is contingent upon the demands of the trajectory and the status of the actuators at the time of failure.

The baseline controller is also observed to perform very well amid the failures. This does not hint at a weakness in the reconfigurable controller, but rather notes a strength in the principles associated with control design in the case of redundant actuators. Also it is important to note that the vehicle maintains stability in large part *because* of this over-actuation: as failures occur, the remaining active actuators are able to decrease the tracking error arising due to the failures.

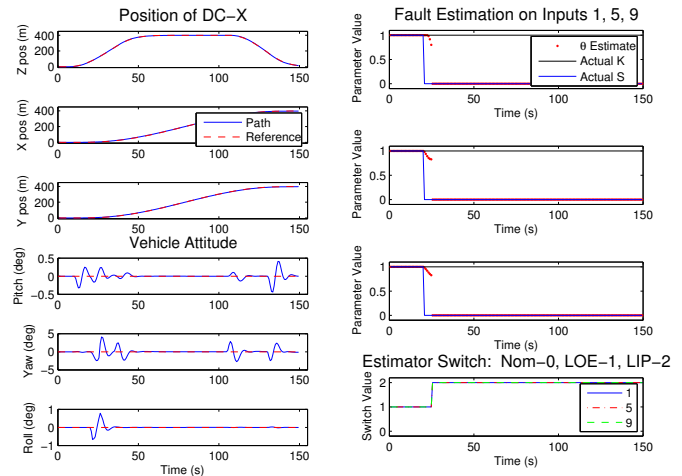
IX. CONCLUSIONS AND FUTURE WORK

In this paper a FDIR control scheme is developed for a dynamic model of the Delta Clipper-Experimental (DC-X) single stage to orbit rocket concept. The six degree of freedom redundantly actuated model provides a well-suited test case for designing a controller for actuators with different response rates using a multiple-model failure parameter estimation method. Even under multiple severe flight-critical failures, the reconfigurable controller was shown through high-fidelity simulations to maintain the desired closed-loop performance. Robustness of the system was demonstrated under a large number of different single and multiple failure cases.

The simulations presented here utilized a linearized controller. Future studies incorporating the dynamic nonlinear controller and a high-fidelity nonlinear plant model are anticipated to provide insight into the capabilities of the proposed system to handle failures in the nonlinear flight regimes and over an enlarged flight envelope. While greater controller and model complexity may provide better tracking over larger failure sets, we note that in the all cases except hard-over failures the linearized reconfigurable controller performed extremely well. Hence a study related to the use of different controllers in different regions of the state or parameter space may be of interest. A suitable framework for the corresponding reconfigurable control design might be based, for instance, on the concept of Multiple Models, Switching and Tuning [10]. Future work will also include a more complete Monte-Carlo simulations to arrive at a precise set of failures that can be accommodated using the proposed approach.

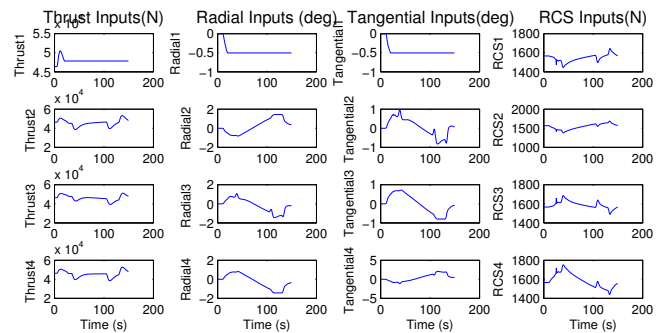
REFERENCES

- [1] "McDonnell Douglas DC-X," http://en.wikipedia.org/wiki/mcdonnell_douglas_dc-x.
- [2] J. Carter, J. Rachel, B. Corbin, R. Block, "Vehicle Management System for Single Stage Rocket," *AIAA, AHS, and ASEE Aerospace Design Conference*, Irvine, CA, Feb. 16-19, 1993.
- [3] S. Voglewede, "Single Stage Rocket Technology's Real Time Data System," NASA. *Goddard Space Flight Center, Third International Symposium on Space Mission Operations and Ground Data Systems Part 1*, pp. 155-168 (SEE N95-17179 04-17), USA, 1994
- [4] D. Nowlan, D. Humphrey, Y. Pak, L. Cook, "Delta Clipper-Experimental (DC-X) GN&C System," *Guidance and Control 1995; Proceedings of the Annual Rocky Mountain Control Conference, Keystone CO*; United States; 1-5 Feb 1995. pp. 527-546. 1995
- [5] J. D. Bošković, J. Redding and R. K. Mehra, "Robust Fault-Tolerant Flight Control using a New Failure Parameterization", in Proc. of *2007 American Control Conference*, New York, July 11-13, 2007.
- [6] J. D. Bošković, R. Prasanth and R. K. Mehra, "Retrofit Reconfigurable Flight Control under Control Effector Damage", *AIAA J. of Guidance, Control & Dynamics*, Vol. 30, No. 3, pp. 703-712, 2007.
- [7] J. D. Bošković, S. E. Bergstrom, R. K. Mehra, J. Urnes, Sr., M. Hood, and Y. Lin, "Fast on-Line Actuator Reconfiguration Enabling (FLARE) System", AIAA-2005-6339, in Proc. of the *2005 AIAA GNC Conference*, San Francisco, CA, August 15-18, 2005.
- [8] J. D. Bošković and R. K. Mehra, "Robust Integrated Flight Control Design Under Failures, Damage and State-Dependent Disturbances", *AIAA J. of Guidance, Control & Dynamics*, Vol. 28, No. 5, 2005.
- [9] J. D. Bošković, L. Chen and R. K. Mehra, "Adaptive Control Design for a Class of Non-Affine Models Arising in Flight Control", *AIAA J. of Guidance, Control & Dynamics*, Vol. 27, No. 2, 2004.
- [10] J. D. Bošković and R. K. Mehra, "A Multiple Model Adaptive Flight Control Scheme for Accommodation of Actuator Failures", *AIAA J. of Guidance, Control & Dynamics*, Vol 25, No. 4, pp. 712-724, 2002.

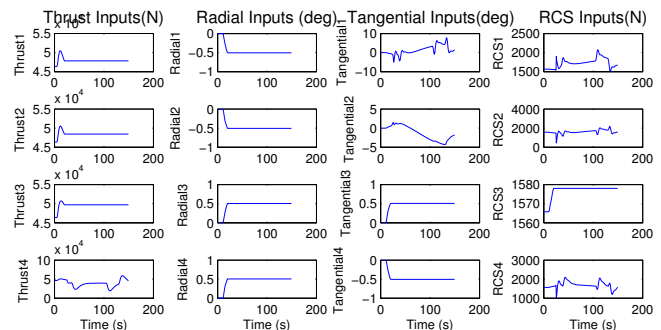


(a) Typical Trajectory with LIP 159

(b) Estimation, LIP 159



(c) Inputs for LIP Failure case at 1,5,9



(d) Inputs for LIP Failure case at 1,2,3,5,6,7,8,11,12,15

Fig. 5. Typical Inputs and Estimates given mild and severe failures.

- [11] M. Bodson and J. Groszkiewicz, "Multivariable Adaptive Algorithms for Reconfigurable Flight Control", *IEEE Transactions on Control Systems Technology*, Vol. 5, No. 2, pp. 217-229, March 1997.
- [12] J. Brinker and K. Wise, "Reconfigurable Flight Control of a Tailless Advanced Fighter Aircraft", in Proc. of the *1998 AIAA GNC Conference*, Vol. 1, pp. 75-87, Boston, MA, August 10-12, 1998.
- [13] A. Calise, S. Lee and M. Sharma, "Direct Adaptive Reconfigurable Control of a Tailless Fighter Aircraft", in Proc. of *1998 AIAA GNC Conference*, Vol. 1, pp. 88-97, Boston, MA, August 10-12, 1998.
- [14] P. Chandler, M. Pachter and M. Mears, "System Identification for Adaptive and Reconfigurable Control", *J. of Guidance, Control & Dynamics*, Vol. 18, No. 3, pp. 516-524, 1995.